

Seebeck coefficient in a nickelate superconductor: electronic dispersion in the strange metal phase

G. Grissonnanche,^{1,2,*} G. A. Pan,³ H. LaBollita,⁴ D. Ferenc Segedin,³ Q. Song,³
H. Paik,^{5,6} C. M. Brooks,³ A. S. Botana,⁴ J. A. Mundy,³ and B. J. Ramshaw^{1,7,†}

¹*Laboratory of Atomic and Solid State Physics, Cornell University, Ithaca, NY, USA*

²*Kavli Institute at Cornell for Nanoscale Science, Ithaca, NY, USA*

³*Department of Physics, Harvard University, Cambridge, MA, USA*

⁴*Department of Physics, Arizona State University, Tempe, AZ, USA*

⁵*Platform for the Accelerated Realization, Analysis,*

and Discovery of Interface Materials, Cornell University, Ithaca, NY, USA

⁶*School of Electrical and Computer Engineering, University of Oklahoma, Norman, OK, USA*

⁷*Canadian Institute for Advanced Research, Toronto, Ontario, Canada*

(Dated: February 3, 2023)

Superconducting nickelates are a new family of materials that combine strongly-correlated magnetism with unconventional superconductivity. While comparisons with the superconducting cuprates are natural, very little is known about the metallic state of the nickelates, making these comparisons difficult. We probe the electronic dispersion of thin-film superconducting 5-layer ($n = 5$) and metallic 3-layer ($n = 3$) nickelates by measuring the Seebeck coefficient, S . We find a temperature independent and negative S/T for both the $n = 5$ nickelate, with strange metal resistivity, and the $n = 3$ compound, with more conventional Fermi liquid resistivity. These results are in stark contrast with the strongly temperature-dependent S/T measured at similar electron filling in the cuprate $\text{La}_{1.36}\text{Nd}_{0.4}\text{Sr}_{0.24}\text{CuO}_4$. We reproduce the temperature dependence, sign, and amplitude of S/T in the nickelates using Boltzmann transport theory combined with the electronic structure calculated from density functional theory. This demonstrates that the electronic structure obtained from first-principles calculations is a good starting point for calculating the transport properties of superconducting nickelates, and suggests that, despite indications of strong electronic correlations, there are well-defined quasiparticles in the metallic state of this family of materials. Finally, we explain the differences in the Seebeck coefficient between nickelates and cuprates as originating in strong dissimilarities in impurity concentrations. Beyond establishing a baseline understanding of how the electronic structure relates to transport coefficients in these new materials, this work demonstrates the power of the semi-classical approach to quantitatively describe transport measurements, even in the strange-metallic state.

PACS numbers: 74.72.Gh, 74.25.Dw, 74.25.F-

I. INTRODUCTION

Unconventional superconductivity remains one of the most active and challenging subfields of strongly correlated electron research, with cuprates posing some of the toughest experimental and theoretical challenges over the past three decades [1]. The origin of high- T_c superconductivity in the cuprates remains a mystery in part due to the complex interplay of several competing states and relatively strong disorder. One approach to understanding the physics of high- T_c is to replace copper entirely, for example with ruthenium or nickel, while maintaining the same square-lattice, transition metal oxide motif. Sr_2RuO_4 is a success of this approach [2], but it does not share the complex phase diagram of the cuprates.

The recent discovery of superconductivity in strontium-doped NdNiO_2 [3–5] and stoichiometric $\text{Nd}_6\text{Ni}_5\text{O}_{12}$ [6] presents an opportunity to explore the key ingredients

for unconventional superconductivity by contrasting the physical properties of the nickelates with the cuprates. The nickelates contain cuprate-like NiO_2 planes, and the family we study here is $\text{Nd}_{n+1}\text{Ni}_n\text{O}_{2n+2}$, where n indicates the number of NiO_2 planes per unit cell [7–11]. While nickel in the $n = \infty$ member of the series— NdNiO_2 —has the same nominal $3d^9$ electronic configuration as copper does in the cuprates, the finite- n members have the nominal configuration of $3d^{9-\delta}$, where $\delta = 1/n$. This offers a mechanism for exploring the hole-doped phase diagram without introducing cation disorder.

Superconducting nickelates exhibit many similarities with the cuprates. These include a phase diagram with a superconducting dome at similar $3d^{8.8}$ electron concentrations, evidence for a nodal superconducting gap [12], magnetism [13, 14], charge density waves [15, 16], and even a strange metal phase [17] (Fig. 1a). Conspicuously absent from this list are experimental comparisons of the electronic structure. To understand which aspects of the electronic dispersion are favorable for unconventional superconductivity, one must first understand how electrons interact in the normal metallic state.

The central difficulty is that most of the experimental

* gael.grissonnanche@cornell.edu

† bradramshaw@cornell.edu

techniques used to study electronic structures are incompatible with current superconducting nickelate samples. There have been attempts to measure the angle-integrated density of states [18], and there are recent angle-resolved photoemission spectroscopy (ARPES) measurements on non-superconducting, single crystal nickelates [19], but ARPES remains out of reach for superconducting nickelate films due to surface quality issues. Similarly, quantum oscillations require metals with a defect density lower than what is currently available in even the cleanest films. This calls for the use of other techniques that are sensitive to the electronic structure and that are compatible with higher levels of elastic scattering from defects and with thin films.

Thermoelectricity—as measured by the Seebeck coefficient S —provides a flexible alternative. Unlike electrical transport, which is only sensitive to the electronic states immediately at the Fermi energy (E_F), the Seebeck effect is sensitive to details of the electronic dispersion away from E_F . Specifically, the Seebeck coefficient reflects the asymmetry of the dispersion above and below E_F —it probes the asymmetry between occupied and unoccupied states, also called particle-hole asymmetry or energy asymmetry [20, 21]. In certain limits—that will be relevant for this study—the Seebeck coefficient becomes independent of the electronic scattering rate, making it a powerful probe of the electronic dispersion. Overall, the Seebeck effect is a complementary transport coefficient to the Hall effect, which reflects the states centered at the Fermi level and which becomes independent of the scattering rate only in the high-field limit.

To investigate the electronic structure of the nickelates, we measure the Seebeck coefficient of a superconducting 5-layer nickelate $\text{Nd}_6\text{Ni}_5\text{O}_{12}$ ($n = 5$ nickelate), whose resistivity is predominantly linear—indicative of strange metal physics (Fig. 7)—as well as a more-overdoped, non-superconducting, 3-layer nickelate $\text{Nd}_4\text{Ni}_3\text{O}_8$ ($n = 3$ nickelate) for comparison (Fig. 1). The 3-layer nickelates have been shown to be one of the closest cuprate analogs to date [22–24]. We find that both the $n = 5$ and $n = 3$ nickelate share a similar temperature independent, negative S/T . We use Boltzmann transport theory to show that the electronic dispersion obtained from first-principles calculations accounts for both the magnitude and sign of the temperature-independent Seebeck coefficient for the two compounds.

To provide a broader context for these results, we compare them to previous measurements of the Seebeck coefficient on the cuprate superconductor $\text{La}_{1.36}\text{Nd}_{0.4}\text{Sr}_{0.24}\text{CuO}_4$ (Nd-LSCO), which has a very similar electron count to the $n = 5$ nickelate (Fig. 1a). At this doping, Nd-LSCO has perfectly T -linear resistivity down to $T = 0$ [25], demonstrating strange metal behavior, and a Seebeck coefficient that is qualitatively different from that of the nickelates. Despite their disparities, we show that the differences in Seebeck coefficients between nickelates and cuprates come from strong dissimilarities in impurity concentrations, and not necessarily from fun-

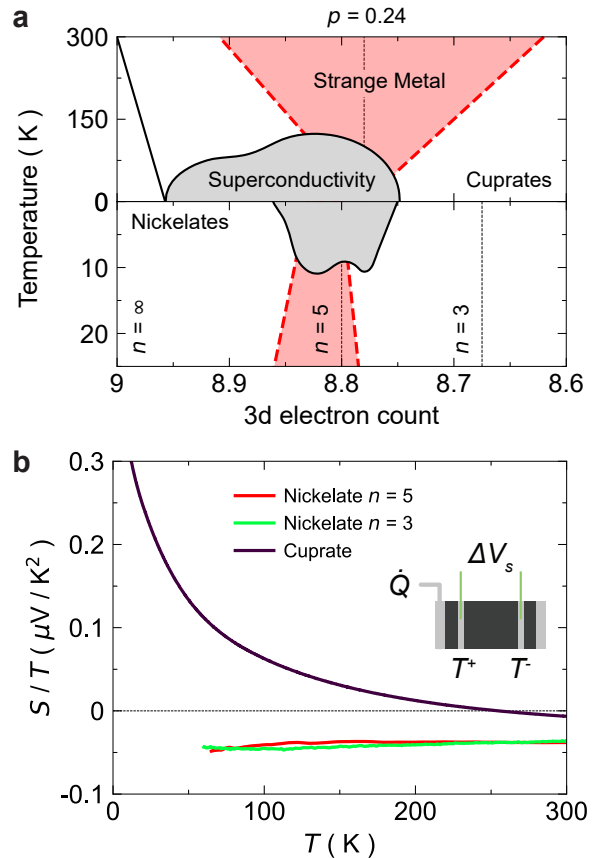


FIG. 1. (a) Schematic temperature versus doping phase diagrams of cuprates (top) and nickelates (bottom). The gray dome indicates the superconducting phase. The red region, delimited by red dashed lines that represent crossover temperature scales, indicates the strange metal regime for both cuprates and nickelates [17]. The vertical black dotted lines represent the electron count for $\text{Nd}_6\text{Ni}_5\text{O}_{12}$ ($\text{Ni}^{1.2+}$: $d^{8.8}$) and $\text{Nd}_4\text{Ni}_3\text{O}_8$ ($\text{Ni}^{1.33+}$: $d^{8.67}$), indicated as $n = 5$ and $n = 3$, respectively. (b) In-plane Seebeck coefficient of $\text{Nd}_6\text{Ni}_5\text{O}_{12}$ ($n = 5$ nickelate), $\text{Nd}_4\text{Ni}_3\text{O}_8$ ($n = 3$ nickelate) and Nd-LSCO $p = 0.24$ (cuprate), plotted as S/T vs T at $B = 0$ T. The inset shows a schematic of the experimental setup. A heater attached to one end of the sample applies a heat current \dot{Q} . The heat current sets up a thermal gradient $\Delta T = T_+ - T_-$, where T_+ (T_-) is the hot (cold) temperature. A voltage drop ΔV_s develops in response to ΔT . The Seebeck coefficient is given by $S = -\Delta V_s / \Delta T$.

damental differences in the nature of the metallic state. These results suggest that, despite the existence of strong electronic correlations, well-defined quasiparticles are responsible for both charge and heat transport in both nickelates and cuprates.

II. METHODS

Samples. The perovskite-like parent $\text{Nd}_{n+1}\text{Ni}_n\text{O}_{3n+1}$ films ($n = 5$ and $n = 3$) were synthesized by molecular

beam epitaxy on (110)-orientated NdGaO_3 . The growth process used distilled ozone, substrate temperatures of $\sim 650\text{--}690^\circ\text{C}$, and the NdNiO_3 calibration procedure described in Ref. [26]. This synthesis was followed by a reduction process contained in a sealed glass ampoule, optimized with a process at $\sim 290^\circ\text{C}$ lasting three hours in order to reach the square-planar $\text{Nd}_{n+1}\text{Ni}_n\text{O}_{2n+2}$ phases (this process is similar to the procedure in Ref. [6]). Using an electron-beam evaporator, contacts consisting of a 10 nm chromium sticking layer and 150 nm of gold were deposited in a Hall bar geometry such that the applied thermal gradient and measured Seebeck voltage were along the [001]-direction of the substrate.

The substrate material NdGaO_3 has a high thermal conductivity that increases 30-fold between room temperature and $\sim 30\text{ K}$ [27], weakening the applied thermal gradient across the nickelate film. To mitigate this effect, we polished the NdGaO_3 substrate to reduce its thickness from 500 microns down to $\sim 100\text{--}150$ microns using diamond lapping film. This served to increase the thermal gradient that generates the Seebeck voltage, which allowed us to measure the Seebeck effect down to $\sim 60\text{ K}$, below which the thermal gradient becomes too small and the experiment cannot be performed reliably. This process necessarily involves a brief heat exposure during sample mounting. We minimized the degradation risk to the sample [28] by using low temperature crystal wax and mounting in an argon glove box; resistivity measurements taken before and after polishing showed no substantial changes.

Measurements. We measured the Seebeck coefficient using an AC technique used previously for cuprates [20]. An AC thermal excitation is generated by passing an electric current at frequency $\omega \sim 0.1\text{ Hz}$ through a 5 k Ω strain gauge used as a heater to generate a thermal gradient in the sample. While the heat is carried primarily by the substrate, this also generates a thermal gradient ΔT_{AC} along the film. We detect this AC thermal gradient at frequency 2ω , as well as the absolute temperature shift, using two type E thermocouples. An AC Seebeck voltage, ΔV_{AC} , is also generated at a frequency 2ω in response to the thermal gradient. We measure this voltage with phosphor-bronze wires attached to the same contacts where the thermocouples measure ΔT_{AC} : this eliminates uncertainties associated with the geometric factor.

The thermocouple and Seebeck voltages were amplified using EM Electronics A10 preamplifiers and detected using a MCL1-540 Synstek lock-in amplifier at the thermal excitation frequency 2ω . The Seebeck coefficient is then given by $S = -\Delta V_{\text{AC}}/\Delta T_{\text{AC}}$. The frequency ω was adjusted so that the thermoelectric voltage and the thermal gradient remained in phase.

Band structure calculations. The paramagnetic electronic structure of the $n = 5$ and $n = 3$ layered nickelates was calculated using density functional theory (DFT) combined with the projector augmented wave method, as implemented in the Vienna *ab-initio* simulation package [29]. We used a pseudopotential that treats the Nd 4f elec-

trons as core electrons. The in-plane lattice parameters were set to match the NdGaO_3 substrate, and we optimized the out-of-plane lattice parameter. See Appendix A for more details on the band structure calculations.

Boltzmann transport. We fit a tight-binding model (Tables I and II) to the DFT band structure and used it to calculate the Seebeck coefficient using Boltzmann transport theory. We applied the same algorithm that was used successfully in the cuprates [20, 30–32] to numerically evaluate the Seebeck coefficient for the nickelates.

III. RESULTS

Seebeck coefficient. To probe the electronic structure of the nickelates, we measured the in-plane Seebeck coefficient. Both nickelate samples, $n = 5$ and $n = 3$, show an S/T that is similar in magnitude, negative, and independent of temperature (Fig. 1b). The Seebeck coefficient of the $n = 5$ layer nickelate is reproduced on a second sample (Appendix C) and the measured one on $n = 3$ is similar to the closely-related 3-layer nickelate $\text{La}_4\text{Ni}_3\text{O}_8$, which also displays a negative Seebeck coefficient above a metal-to-insulator transition at 105 K [33]. However, this contrasts with the cuprate Nd-LSCO $p = 0.24$, whose Seebeck coefficient is strongly temperature dependent and changes sign near room temperature (Fig. 1b).

Boltzmann calculations. We performed Boltzmann transport calculations to interpret the (lack of) temperature dependence and the negative sign of S/T in both the $n = 5$ and $n = 3$ nickelates (see Appendix B for more details). For a free-electron model (i.e. a circular Fermi surface), the sign of the Seebeck coefficient reflects the sign of the charge carriers—hole (positive) or electron (negative)—which is similar to the Hall coefficient. For a real material, the Seebeck coefficient is sensitive to the particle-hole asymmetry of the electronic dispersion, as well as the particle-hole asymmetry of the scattering rate, and the resulting Seebeck coefficient can be of either sign.

We obtain good agreement between the calculated and measured S/T for the nickelates by using a tight-binding fit to the DFT and a constant (energy and temperature independent) scattering rate, $1/\tau_0$ (Fig. 2a, b).

In contrast, energy-dependent scattering is a key ingredient for reproducing S/T in the cuprate Nd-LSCO at $p = 0.24$. Indeed, the agreement between the cuprate data and Boltzmann calculations, reproduced in Fig. 2f from Gourgout et al. [20], was achieved by invoking an inelastic particle-hole asymmetric scattering rate. This means that the scattering rate is not only energy dependent in the cuprate, but it is also linear-in-energy with a different slope above and below the Fermi energy, here labeled $1/\tau_{\text{asym}}(\epsilon)$ (see Appendix B and Gourgout et al. [20] for more details).

Effect of impurity scattering. The stark difference in S/T between the nickelates and cuprates is somewhat surprising given the similarity of their electronic structures. Both compounds have predominantly $3d^9$ bands

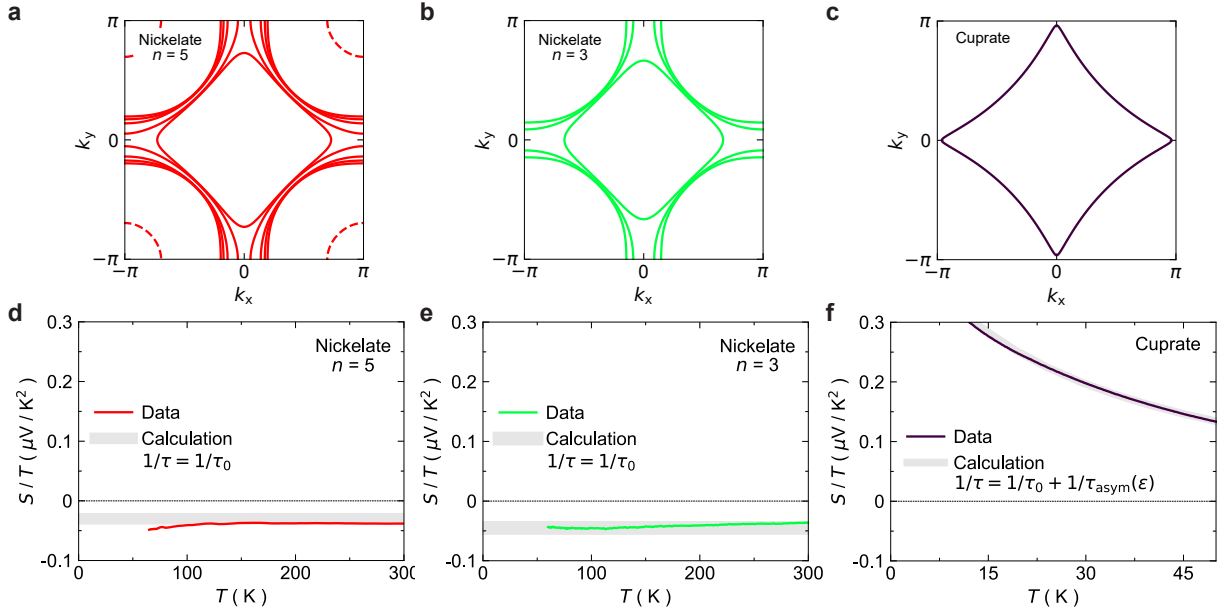


FIG. 2. Fermi surfaces and Seebeck coefficient plotted as S/T vs T for (a, d) $\text{Nd}_6\text{Ni}_5\text{O}_{12}$ ($n = 5$ nickelate); (b, e) $\text{Nd}_4\text{Ni}_3\text{O}_8$ ($n = 3$ nickelate); (c, f) Nd-LSCO $p = 0.24$ (cuprate). The Fermi surface for the $n = 5$ nickelate includes 5 sheets of $d_{x^2-y^2}$ character (1 electron-like, 4 hole like) centered around $(0,0)$ and one Nd-d sheet (dashed) centered at the zone corner. For the $n = 3$ nickelate, there are 3 sheets of $d_{x^2-y^2}$ (1 electron-like, 2 hole-like). Panels (d) and (e) compare the measured Seebeck coefficient to the one calculated from DFT using Boltzmann transport and a constant elastic scattering rate $1/\tau_0$. The calculation for Nd-LSCO $p = 0.24$, panel (f), uses the sum of an elastic scattering rate $1/\tau_0$ and a particle-hole asymmetric scattering rate, $1/\tau_{\text{asym}}(\epsilon)$, as described in Gourgout et al. [20].

crossing the Fermi energy, and the curvatures of the Fermi surfaces are not all that different—the single Fermi surface in Nd-LSCO essentially interpolates between the hole and electron-like Fermi surfaces found in the multi-layer nickelates (Fig. 2a, b, c). Given that the band structure is largely temperature-independent, the disparities in S/T between the two families must originate in a difference in the scattering rate.

To understand this difference, we examine the relative amounts of disorder in the cuprate and nickelate samples by comparing the residual resistivities, ρ_0 . For the $n = 5$ and $n = 3$ nickelates, $\rho_0 = 1450 \mu\Omega \text{ cm}$ and $920 \mu\Omega$ respectively (Pan et al. [6]), which is significantly larger than the $\rho_0 = 23 \mu\Omega \text{ cm}$ of Nd-LSCO $p = 0.24$ [25]. Using Boltzmann transport, we estimate from ρ_0 that the elastic scattering rate, $1/\tau_0$, is approximately 350 times higher for the $n = 5$ nickelate, and 180 times for $n = 3$, compared to Nd-LSCO $p = 0.24$ ($1/\tau_0 = 10 \text{ ps}^{-1}$).

In the limit where the scattering rate is predominately energy-independent (elastic), the Seebeck coefficient becomes independent of scattering because it is the ratio two quantities that are inversely proportional to the scattering rate: the Peltier coefficient $\alpha \propto \tau_0$ and the electric conductivity $\sigma \propto \tau_0$. The measured temperature-independent S/T in the nickelates suggests that the elastic scattering is indeed dominant, whereas inelastic scattering must contribute strongly for the cuprate.

To confirm this picture, we increase the relative amount of elastic scattering to inelastic scattering in our model

of the cuprate and show that S/T becomes temperature independent. Increasing $1/\tau_0 = 10 \text{ ps}^{-1}$ to 3500 ps^{-1} while holding $1/\tau_{\text{asym}}(\epsilon)$ fixed, we change the calculated S/T for the cuprate to a temperature-independent, negative value—very similar to what we measured in the nickelates (Fig. 3). This confirms that the nickelate films are dominated by elastic scattering and, in this limit, S/T directly reflects the particle-hole asymmetry of the bands rather than the energy dependence of the scattering rate. Note that the elastic scattering rate in the infinite layer nickelates is about 10 times smaller [17] than in the $n = 5$ nickelate. However, Fig. 6 shows that the infinite layer nickelates are still in the limit where the elastic scattering rate dominates over the energy-asymmetric scattering and thus should also exhibit a negative and temperature-independent Seebeck coefficient.

IV. DISCUSSION

Scattering rate. The positive Seebeck coefficient measured in overdoped cuprates remained a puzzle for decades [21]. Boltzmann transport calculations using the band structure obtained from ARPES [34] and the scattering rates obtained from angle dependent magnetoresistance (ADMR) [30] gave values of S/T for the cuprate similar to what is measured in $n = 5$ and $n = 3$ nickelates, but which were very far from the experimental data [20]. This

puzzle was resolved by incorporating energy-dependent, particle-hole asymmetric scattering rate into the model (an ansatz that was supported by theoretical calculations using a non-Fermi-liquid self-energy [35]).

In contrast, we do not need to invoke an energy-dependent scattering rate to reproduce the data in the nickelates—the particle-hole asymmetry of the electronic dispersion itself is sufficient. This is because the large elastic scattering in the nickelate films dominates over any other scattering process. As a consequence, we cannot exclude that such energy-dependent scattering exists in the nickelates, but it would require thin films with a lower amount of elastic scattering from defects to observe. Fortunately, what the larger level of elastic disorder does is make the Seebeck coefficient only sensitive to the band dispersion and not to the scattering rate at all—similar to the high-field limit of the Hall coefficient, the high-elastic-scattering limit of S/T reflects only the underlying band dispersion.

Two assumptions go into the Boltzmann calculations that have quantitative effects on the calculated value of S/T . First, we assume that the scattering rate is the same on all bands. Because the Fermi velocity is of a similar magnitude on all bands, and because the strong elastic scattering is likely dominated by impurities that fix a real-space mean free path, it is reasonable to assume that the elastic mean free path is similar on all bands. This assumption introduces some uncertainty into the absolute value of S/T but does not change it qualitatively as long as the scattering is not radically different (e.g. smaller by a factor of 10 or more) on one of the bands.

Second, we assume that the bandwidth calculated by DFT is the correct one. In real materials, electron-electron interactions tend to lower the overall bandwidth, which in turn reduces our tight-binding bandwidth t and thus increases the calculated $|S/T|$. While a proper measurement of the bandwidth is not available for these films, it is known that DFT has overestimated the bandwidth in lanthanum-based cuprates by about a factor of 2 [30, 36]. We incorporate a factor of 2 uncertainty in the bandwidth into our calculated S/T in Fig. 2d and e.

Strange metal. Strange metallicity has been reported in the region of the phase diagram where the 5-layer superconducting nickelate is located in doping [17] (Fig. 1a). While the resistivity of the $n = 5$ nickelate is not fully linear in temperature, its temperature dependence can be written as $aT + bT^2$ (Fig. 7) with a dominant T -linear component, locating the $n = 5$ nickelate in the strange metal phase. It is therefore even more surprising that we can describe the thermoelectric transport of the nickelates using standard, semi-classical Boltzmann transport, when other theories have predicted the absence of well-defined quasiparticles [37]. This is in line with many recent studies in cuprates that have demonstrated the validity of the semi-classical approach for calculating transport in strange metals [20, 30–32] and Fermi liquids [38]. In the case of the nickelates, this not only surprisingly confirms the physical realization of the predictions from DFT—

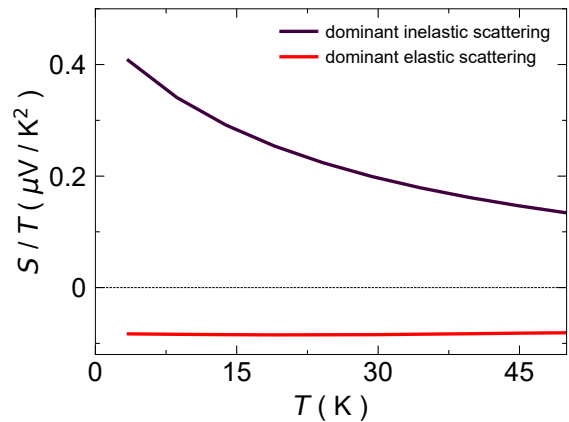


FIG. 3. Calculated Seebeck coefficient, plotted as S/T of Nd-LSCO $p = 0.24$ in the limits of dominant inelastic scattering rate ($1/\tau_0 \sim 1/\tau_{\text{asym}}(\epsilon)$) and dominant elastic scattering ($1/\tau_0 \gg 1/\tau_{\text{asym}}(\epsilon)$). In both cases, the total scattering rate is given by the $1/\tau_0 + 1/\tau_{\text{asym}}(\epsilon)$. In the “clean” limit (purple), we use the elastic scattering rate extracted from ADMR [30] on Nd-LSCO $p = 0.24$, which gives $1/\tau_0 = 10 \text{ ps}^{-1}$. In the dirty limit (red), we use the elastic scattering rate extracted from the residual resistivity of the $n = 5$ nickelate, which is $1/\tau_0 = 3500 \text{ ps}^{-1}$.

despite the correlated electronic state of these materials—it also demonstrates the reliability of Boltzmann theory to describe the transport properties of unconventional superconductors such as the nickelates.

V. SUMMARY

We report the first thermoelectric study of a superconducting nickelate. We use the Seebeck effect to probe the electronic dispersion of both a superconducting and strange metal 5-layer nickelate, as well as a metallic, 3-layer nickelate. We compare the measured Seebeck coefficient to semi-classical transport calculations using electronic dispersions from first-principal calculations. We find that the calculated S/T reproduces the amplitude, sign, and temperature dependence of the measured Seebeck coefficient. We compare our nickelate measurements to those of the cuprate Nd-LSCO at $p = 0.24$ —a strange metal—and find qualitative disagreement despite similarities in the electronic structure of the families. We show that the higher level of disorder present in the nickelate thin films compared to the single-crystal cuprates explains this discrepancy. In this limit, the Seebeck effect turns out to be a powerful, scattering-rate independent probe of the electronic structure.

Our results suggest that both semi-classical transport theory and DFT are reliable means for predicting and understanding the transport properties of the nickelates, even in proximity to a strange-metal state. These results also demonstrate the advantage of thermoelectric measurements combined with theoretical tools to probe

the electronic dispersion—the same way these tools were used successfully in the cuprates [20, 30–32]. These recent successes of uniting theory with experiments to extract fundamental information about the electrons from transport measurements will open a new path to describing the normal state from which unconventional superconductivity emerges.

ACKNOWLEDGMENTS

B.J.R. and G.G. acknowledge funding from the Department of Energy under grant no. DE-SC0019331. G.A.P. and D.F.S. are primarily supported by U.S. Department of Energy (DOE), Office of Basic Energy Sciences, Division of Materials Sciences and Engineering, under Award No. DE-SC0021925; and by NSF Graduate Research Fellowship Grant No. DGE-1745303. G.A.P. acknowledges additional support from the Paul & Daisy Soros Fellowship for New Americans. Q.S. was supported by the Science and Technology Center for Integrated Quantum Materials, NSF Grant No. DMR-1231319. J.A.M. acknowledges support from the Packard Foundation and the Gordon and Betty Moore Foundation’s EPiQS Initiative, Grant No. GBMF6760. Materials growth was supported by PARADIM under National Science Foundation (NSF) Cooperative Agreement No. DMR-2039380. We acknowledge the Cornell LASSP Professional Machine Shop for their contributions to designing and fabricating equipment used in this study. H.L. and A.S.B. acknowledge the support from NSF Grant No. DMR 2045826, the ASU Research Computing Center and the Extreme Science and Engineering Discovery Environment (XSEDE) through research allocation TG-PHY220006, which is supported by NSF grant number ACI-1548562 for HPC resources.

Appendix A: DFT Computational Details

Density-functional theory calculations for the $n = 5$ and $n = 3$ nickelates were performed using the projector augmented plane-wave method as implemented in the VASP code [29]. For the exchange-correlation functional, we have used the Perdew-Burke-Ernzerhof (PBE) version of the generalized gradient approximation [39]. The reduced Ruddlesden-Popper nickelates crystallize in a tetragonal structure where we have fixed the in-plane lattice constants to match those of the NdGaO_3 substrate. The out-of-plane lattice constants were optimized and agree with the experimental values, namely $c = 25.4 \text{ \AA}$ and $c = 38.8 \text{ \AA}$ for the $n = 5$ and $n = 3$ materials, respectively [6]. The size of our plane-wave basis is determined by an energy cutoff of $E_{\text{cut}} = 500 \text{ eV}$ and integration in the Brillouin zone is performed on a $12 \times 12 \times 12$ k -mesh for both materials.

Figure 4 provides a brief summary of the paramagnetic electronic structure of the $n = 5$ and $n = 3$ nickelates. The band structures reveal a $d_{x^2-y^2}$ band per NiO_2 layer

Band	μ/t	t (meV)	t'/t	t''/t
Ni 1	-1.101	396.6	-0.1833	0.1042
Ni 2	-1.216	400.5	-0.1458	0.0855
Ni 3	-0.765	420.9	-0.2597	0.1075
Ni 4	-0.839	425.1	-0.2483	0.0947
Ni 5	-0.906	417.1	-0.2297	0.0795
Nd	3.157	380.0	0	0

TABLE I. Tight-binding parameters from the bands of $n = 5$ nickelate obtained from a fit to the band dispersion calculated by DFT [26].

Band	μ/t	t (meV)	t'/t	t''/t
Ni 1	-1.384	410.4	-0.1532	0.0719
Ni 2	-1.037	426.2	-0.2505	0.1071
Ni 3	-1.138	422.1	-0.2205	0.0988

TABLE II. Tight-binding parameters from the bands of $n = 3$ nickelate obtained from a fit to the band dispersion calculated by DFT [26].

crossing the Fermi energy (E_F), akin to the multi-layer cuprates. Interestingly, for the 5-layer nickelate, there are additional electron pockets at the Brillouin zone corners (M and A) coming from the rare-earth bands. For the 3-layer material, these “spectator” bands sit above E_F . Indeed, the orbital-resolved density of states (DOS) reveals the dominant states are of $\text{Ni-}d_{x^2-y^2}$ character around the E_F . The $\text{Ni-}d_{z^2}$ and $\text{Ni-}t_{2g}$ ($t_{2g} \equiv \{d_{xy}, d_{xz}, d_{yz}\}$) states are positioned well below E_F and do not play a significant role in the low-energy physics of these materials. For a complete description of the electronic structure of the reduced Ruddlesden-Popper nickelates, see Refs. 10 and 11.

Appendix B: Boltzmann calculations

The Seebeck coefficient is given by the ratio of the Peltier coefficient α_{ii} to the electrical conductivity σ_{ii} (with $i = x, z$), $S_i = \alpha_{ii}/\sigma_{ii}$, where

$$\sigma_{ii} = \int_{-\infty}^{\infty} d\epsilon \left(-\frac{\partial f(\epsilon)}{\partial \epsilon} \right) \sigma_{ii}(\epsilon) \quad (\text{B1})$$

$$\alpha_{ii} = \int_{-\infty}^{\infty} d\epsilon \left[\left(-\frac{\partial f(\epsilon)}{\partial \epsilon} \right) \frac{\epsilon}{T} \right] \frac{\sigma_{ii}(\epsilon)}{-e} \quad (\text{B2})$$

with e the electron charge, $f(\epsilon)$ the Fermi-Dirac distribution and

$$\sigma_{ii}(\epsilon) = 2e^2 \iiint_{\text{BZ}} \frac{d^3k}{(2\pi)^3} v_i(\vec{k})^2 \tau(\vec{k}, \epsilon) \delta(\epsilon - E(\vec{k})), \quad (\text{B3})$$

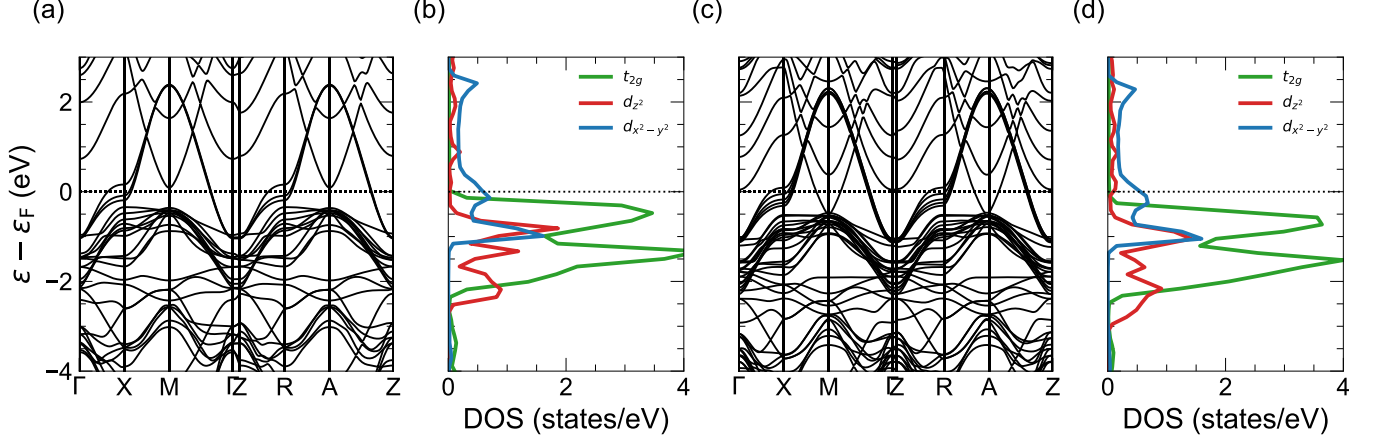


FIG. 4. (a) Band structure and (b) orbital-resolved density of states for the Ni(3d) shell within DFT for the tri-layer nickelate ($n = 3$). (c,d) same as (a,b) for the quintuple-layer nickelate ($n = 5$), respectively.

where $v_i(\vec{k})$ is the component of the quasiparticle velocity in the i -direction, $\tau(\vec{k}, \epsilon)$ is the quasiparticle lifetime depending on both momentum \vec{k} and energy ϵ , and $E(\vec{k})$ is given by a tight-binding model.

In order to calculate Seebeck coefficient of the $n = 5$ and $n = 3$ nickelates, we fitted a tight-binding model $E(\vec{k})$ to the band dispersion calculated by DFT with

$$E(\vec{k}) = -\mu - 2t[\cos(k_x a) + \cos(k_y a)] - 4t' \cos(k_x a) \cos(k_y a) - 2t''[\cos(2k_x a) + \cos(2k_y a)] \quad (\text{B4})$$

with $a = 3.91 \text{ \AA}$ (3.86 \AA) and $c = 38.8 \text{ \AA}$ (25.4 \AA) the lattice constants for the $n = 5$ ($n = 3$) nickelate. The hopping parameters are found in the tables I and II.

Appendix C: Sample comparison of $n = 5$ nickelates

Here we compare the Seebeck coefficient of two samples of $n = 5$ nickelate (Fig. 5). The superconducting sample was only measured down to 100 kelvin due to having a thicker substrate, which made it impossible within the temperature resolution to generate a sizable thermal gradient below that 100 kelvin to measure the Seebeck effect. Indeed, the thermal conductivity of the substrate, NdGaO₃, increases dramatically at low temperature, short-circuiting any attempt to generate a thermal gradient with a reasonable amount of heat. The second sample was grown in similar conditions, but did not exhibit superconductivity due to the sensitivity of the superconducting state to few percent changes in the cation stoichiometry. We were able to reduce the thickness of that sample substrate down to 150 microns to be able to measure the Seebeck effect down to lower temperature $\approx 60 \text{ K}$ on this sample. Fortunately, the Seebeck coefficients between the two samples are very similar and agree

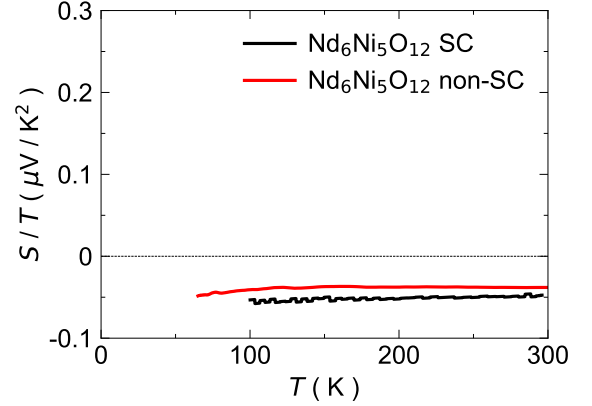


FIG. 5. S/T as a function of temperature of two different $n = 5$ nickelate samples. The first sample is a superconducting nickelate thin film with a substrate thickness of 500 microns. The non-superconducting nickelate has a reduced substrate thickness down to 150 microns.

to within 15%. This difference may be accounted for by the varying levels of cation disorder introduced during the MBE-synthesis of the two samples, as well as by the randomness inherent to the chemical reduction process used in the synthesis of all square-planar nickelates. Nevertheless, the overall reproducibility confirms that the normal state is similar between these samples.

Appendix D: Rare-earth band

One significant difference between the two nickelates is the presence of a neodymium band crossing the Fermi level for the superconducting, 5-layer nickelate. The role of this band is unknown—whether it contributes significantly to the conductivity, or even to the superconducting pairing [40]. To include the neodymium band in the Boltzmann transport calculations changes from $S/T =$

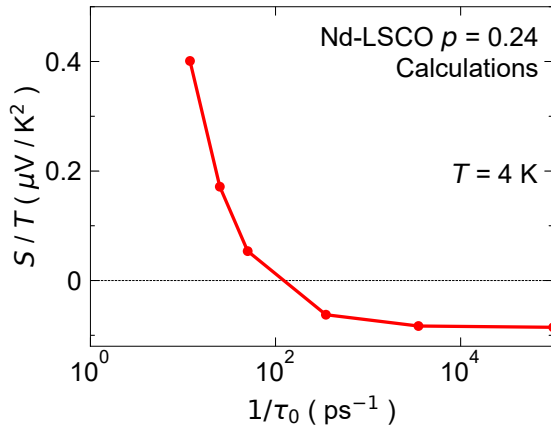


FIG. 6. Calculated Seebeck coefficient, plotted as S/T of Nd-LSCO $p = 0.24$ as a function of elastic scattering rate at $T = 4$ K. The total scattering rate is given by the $1/\tau_0 + 1/\tau_{\text{asym}}(\epsilon)$.

-26.4 nV / K² with it to $S/T = -32.8$ nV / K² without. This 20% difference is likely to remain undetected within the experimental error bars. Therefore, it is difficult to conclude whether the rare-earth band participates in the measured Seebeck coefficient as calculations indicate its contribution remains marginal. This could suggest that the neodymium band does not play a dominant role in the metallic state of the 5-layer superconducting nickelate,

which in turn suggests that it may not play a role in the superconductivity.

Appendix E: Elastic scattering dependence

In the calculations of the Seebeck coefficient of Nd-LSCO $p = 0.24$, the total scattering rate by $1/\tau = 1/\tau_0 + 1/\tau_{\text{asym}}(\epsilon)$. The Seebeck coefficient changes from positive at small values of $1/\tau_0$ to negative and independent of the elastic scattering rate for larger values $1/\tau_0$ as shown in Fig. 6.

Appendix F: Resistivity of the nickelates

The resistivity of the $n = 5$ nickelate includes a significant T -linear component, a synonym of strange metallicity and can be described by $\rho(T) = \rho_0 + a_1T + a_2T^2$ as shown in Fig. 7a, with values $\rho_0 = 1450$ $\mu\Omega\text{cm}$, $a_1 = 8.1$ $\mu\Omega\text{cm} / \text{K}$, and $a_2 = 0.0695$ $\mu\Omega\text{cm} / \text{K}^2$.

However, the resistivity of the $n = 3$ nickelate is purely T^2 , as expected for a Fermi liquid and in the more overdoped region of the phase diagram. In this case, $\rho(T) = \rho_0 + a_1T + a_2T^2$ as shown in Fig. 7b, with values $\rho_0 = 920$ $\mu\Omega\text{cm}$, $a_1 = 0.1$ $\mu\Omega\text{cm} / \text{K}$, and $a_2 = 0.0739$ $\mu\Omega\text{cm} / \text{K}^2$.

- [1] B. Keimer, S. A. Kivelson, M. R. Norman, S. Uchida, and J. Zaanen, From quantum matter to high-temperature superconductivity in copper oxides, *Nature* **518**, 179 (2015).
- [2] Y. Maeno, H. Hashimoto, K. Yoshida, S. Nishizaki, T. Fujita, J. G. Bednorz, and F. Lichtenberg, Superconductivity in a layered perovskite without copper, *Nature* **372**, 10.1038/372532a0 (1994).
- [3] D. Li, K. Lee, B. Y. Wang, M. Osada, S. Crossley, H. R. Lee, Y. Cui, Y. Hikita, and H. Y. Hwang, Superconductivity in an infinite-layer nickelate, *Nature* **572**, 624 (2019).
- [4] D. Li, B. Y. Wang, K. Lee, S. P. Harvey, M. Osada, B. H. Goodge, L. F. Kourkoutis, and H. Y. Hwang, Superconducting dome in $\text{Nd}_{1-x}\text{Sr}_x\text{NiO}_2$ infinite layer films, *Phys. Rev. Lett.* **125**, 027001 (2020).
- [5] S. Zeng, C. S. Tang, X. Yin, C. Li, M. Li, Z. Huang, J. Hu, W. Liu, G. J. Omar, H. Jani, Z. S. Lim, K. Han, D. Wan, P. Yang, S. J. Pennycook, A. T. S. Wee, and A. Ariando, Phase diagram and superconducting dome of infinite-layer $\text{Nd}_{1-x}\text{Sr}_x\text{NiO}_2$ thin films, *Phys. Rev. Lett.* **125**, 147003 (2020).
- [6] G. A. Pan, D. Ferenc Segedin, H. LaBollita, Q. Song, E. M. Nica, B. H. Goodge, A. T. Pierce, S. Doyle, S. Novakov, D. Córdova Carrizales, A. T. N'Diaye, P. Shafer, H. Paik, J. T. Heron, J. A. Mason, A. Yacoby, L. F. Kourkoutis, O. Erten, C. M. Brooks, A. S. Botana, and J. A. Mundy, Superconductivity in a quintuple-layer square-planar nickelate, *Nature Materials* **21**, 160 (2022).
- [7] V. V. Poltavets, K. A. Lokshin, M. Croft, T. K. Mandal, T. Egami, and M. Greenblatt, Crystal structures

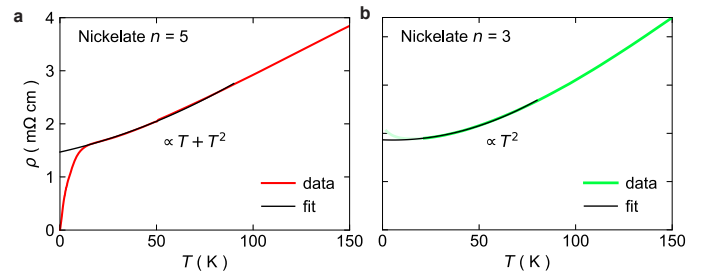


FIG. 7. Resistivity ρ as a function of temperature for (a) $n = 5$ nickelate and (b) $n = 3$ nickelate in $B = 0$. The faded upturn part of the resistivity for $n = 3$ betrays signatures of weak localization due to disorder at low temperature and was not part of the fit.

of $\text{Ln}_4\text{Ni}_3\text{O}_8$ ($\text{Ln} = \text{La, Nd}$) triple layer t' -type nickelates, *Inorganic Chemistry* **46**, 10887 (2007).

- [8] V. V. Poltavets, M. Greenblatt, G. H. Fecher, and C. Felser, Electronic properties, band structure, and fermi surface instabilities of $\text{Ni}^{1+}/\text{Ni}^{2+}$ nickelate $\text{La}_3\text{Ni}_2\text{O}_6$, iso-electronic with superconducting cuprates, *Phys. Rev. Lett.* **102**, 046405 (2009).
- [9] V. V. Poltavets, K. A. Lokshin, A. H. Nevidomskyy, M. Croft, T. A. Tyson, J. Hadernmann, G. Van Tendeloo, T. Egami, G. Kotliar, N. ApRoberts-Warren, A. P. Dio-guardi, N. J. Curro, and M. Greenblatt, Bulk magnetic

- order in a two-dimensional $\text{Ni}^{1+}/\text{Ni}^{2+}$ (d^9/d^8) nickelate, isoelectronic with superconducting cuprates, *Phys. Rev. Lett.* **104**, 206403 (2010).
- [10] H. LaBollita and A. S. Botana, Electronic structure and magnetic properties of higher-order layered nickelates: $\text{La}_{n+1}\text{Ni}_n\text{O}_{2n+2}$ ($n = 4 - 6$), *Phys. Rev. B* **104**, 035148 (2021).
- [11] H. LaBollita, M.-C. Jung, and A. S. Botana, Many-body electronic structure of $d^{9-\delta}$ layered nickelates, *Phys. Rev. B* **106**, 115132 (2022).
- [12] A. Botana and M. Norman, Similarities and differences between LaNiO_2 and CaCuO_2 and implications for superconductivity, *Physical Review X* **10**, 011024 (2020).
- [13] H. Lu, M. Rossi, A. Nag, M. Osada, D. F. Li, K. Lee, B. Y. Wang, M. Garcia-Fernandez, S. Agrestini, Z. X. Shen, E. M. Been, B. Moritz, T. P. Devereaux, J. Zaanen, H. Y. Hwang, K.-J. Zhou, and W. S. Lee, Magnetic excitations in infinite-layer nickelates, *Science* **373**, 213 (2021), publisher: American Association for the Advancement of Science.
- [14] J. Fowlie, M. Hadjimichael, M. M. Martins, D. Li, M. Osada, B. Y. Wang, K. Lee, Y. Lee, Z. Salman, T. Prokscha, J.-M. Triscone, H. Y. Hwang, and A. Suter, Intrinsic magnetism in superconducting infinite-layer nickelates, *Nature Physics* **18**, 1043 (2022), arXiv:2201.11943.
- [15] M. Rossi, M. Osada, J. Choi, S. Agrestini, D. Jost, Y. Lee, H. Lu, B. Y. Wang, K. Lee, A. Nag, Y.-D. Chuang, C.-T. Kuo, S.-J. Lee, B. Moritz, T. P. Devereaux, Z.-X. Shen, J.-S. Lee, K.-J. Zhou, H. Y. Hwang, and W.-S. Lee, A broken translational symmetry state in an infinite-layer nickelate, *Nature Physics* **18**, 869 (2022).
- [16] C. C. Tam, J. Choi, X. Ding, S. Agrestini, A. Nag, M. Wu, B. Huang, H. Luo, P. Gao, M. García-Fernández, L. Qiao, and K.-J. Zhou, Charge density waves in infinite-layer NdNiO_2 nickelates, *Nature Materials* **21**, 1116 (2022).
- [17] K. Lee, B. Y. Wang, M. Osada, B. H. Goodge, T. C. Wang, Y. Lee, S. Harvey, W. J. Kim, Y. Yu, C. Murthy, S. Raghu, L. F. Kourkoutis, and H. Y. Hwang, Character of the "normal state" of the nickelate superconductors (2022), arXiv:2203.02580.
- [18] Z. Chen, M. Osada, D. Li, E. M. Been, S.-D. Chen, M. Hashimoto, D. Lu, S.-K. Mo, K. Lee, B. Y. Wang, F. Rodolakis, J. L. McChesney, C. Jia, B. Moritz, T. P. Devereaux, H. Y. Hwang, and Z.-X. Shen, Electronic structure of superconducting nickelates probed by resonant photoemission spectroscopy, *Matter* **5**, 1806 (2022).
- [19] H. Li, P. Hao, J. Zhang, K. Gordon, A. G. Linn, H. Zheng, X. Zhou, J. F. Mitchell, and D. S. Dessau, Electronic structure and correlations in planar trilayer nickelate $\text{Pr}_4\text{Ni}_3\text{O}_8$, arXiv:2207.13633 10.48550/arXiv.2207.13633 (2022).
- [20] A. Gourgout, G. Grissonnanche, F. Laliberté, A. Ataei, L. Chen, S. Verret, J.-S. Zhou, J. Mravlje, A. Georges, N. Doiron-Leyraud, and L. Taillefer, Seebeck coefficient in a cuprate superconductor: Particle-hole asymmetry in the strange metal phase and fermi surface transformation in the pseudogap phase, *Physical Review X* **12**, 011037 (2022).
- [21] T. Kondo, T. Takeuchi, U. Mizutani, T. Yokoya, S. Tsuda, and S. Shin, Contribution of electronic structure to thermoelectric power in $(\text{Bi,Pb})_2(\text{Sr,Lu})_2\text{CuO}_{6+\delta}$, *Physical Review B* **72**, 024533 (2005).
- [22] J. Zhang, Y.-S. Chen, D. Phelan, H. Zheng, M. R. Norman, and J. F. Mitchell, Stacked charge stripes in the quasi-2d trilayer nickelate $\text{La}_4\text{Ni}_3\text{O}_8$, *Proceedings of the National Academy of Sciences* **113**, 8945 (2016).
- [23] J. Zhang, A. S. Botana, J. W. Freeland, D. Phelan, H. Zheng, V. Pardo, M. R. Norman, and J. F. Mitchell, Large orbital polarization in a metallic square-planar nickelate, *Nature Physics* **13**, 864 (2017).
- [24] S. Sarkar, I. Dasgupta, M. Greenblatt, and T. Saha-Dasgupta, Electronic and magnetic structures of bilayer $\text{La}_3\text{Ni}_2\text{O}_6$ and trilayer $\text{La}_4\text{Ni}_3\text{O}_8$ nickelates from first principles, *Phys. Rev. B* **84**, 180411 (2011).
- [25] R. Daou, N. Doiron-Leyraud, D. LeBoeuf, S. Y. Li, F. Laliberté, O. Cyr-Choinière, Y. J. Jo, L. Balicas, J.-Q. Yan, J.-S. Zhou, J. B. Goodenough, and L. Taillefer, Linear temperature dependence of resistivity and change in the fermi surface at the pseudogap critical point of a high- T_c superconductor, *Nature Physics* **5**, 31 (2009).
- [26] G. A. Pan, Q. Song, D. Ferenc Segedin, M.-C. Jung, H. El-Sherif, E. E. Fleck, B. H. Goodge, S. Doyle, D. Córdoba Carrizales, A. T. N'Diaye, P. Shafer, H. Paik, L. F. Kourkoutis, I. El Baggari, A. S. Botana, C. M. Brooks, and J. A. Mundy, Synthesis and electronic properties of $\text{Nd}_{n+1}\text{Ni}_n\text{O}_{3n+1}$ Ruddlesden-Popper nickelate thin films, *Phys. Rev. Materials* **6**, 055003 (2022).
- [27] W. Schnelle, R. Fischer, and E. Gmelin, Specific heat capacity and thermal conductivity of NdGaO_3 and LaAlO_3 single crystals at low temperatures, *Journal of Physics D: Applied Physics* **34**, 846 (2001).
- [28] X. Ding, S. Shen, H. Leng, M. Xu, Y. Zhao, J. Zhao, X. Sui, X. Wu, H. Xiao, X. Zu, B. Huang, H. Luo, P. Yu, and L. Qiao, Stability of superconducting $\text{Nd}_{0.8}\text{Sr}_{0.2}\text{NiO}_2$ thin films, *Science China Physics, Mechanics & Astronomy* **65**, 267411 (2022).
- [29] G. Kresse and J. Furthmüller, Efficient iterative schemes for ab initio total-energy calculations using a plane-wave basis set, *Phys. Rev. B* **54**, 11169 (1996).
- [30] G. Grissonnanche, Y. Fang, A. Legros, S. Verret, F. Laliberté, C. Collignon, J. Zhou, D. Graf, P. A. Goddard, L. Taillefer, and B. J. Ramshaw, Linear-in temperature resistivity from an isotropic planckian scattering rate, *Nature* **595**, 667 (2021).
- [31] Y. Fang, G. Grissonnanche, A. Legros, S. Verret, F. Laliberté, C. Collignon, A. Ataei, M. Dion, J. Zhou, D. Graf, M. J. Lawler, P. A. Goddard, L. Taillefer, and B. J. Ramshaw, Fermi surface transformation at the pseudogap critical point of a cuprate superconductor, *Nature Physics* **18**, 558 (2022).
- [32] A. Ataei, A. Gourgout, G. Grissonnanche, L. Chen, J. Baglo, M.-E. Boulanger, F. Laliberté, S. Badoux, N. Doiron-Leyraud, V. Oliviero, S. Benhabib, D. Vignolles, J.-S. Zhou, S. Ono, H. Takagi, C. Proust, and L. Taillefer, Electrons with Planckian scattering obey standard orbital motion in a magnetic field, *Nature Physics* , 1 (2022), publisher: Nature Publishing Group.
- [33] J.-G. Cheng, J.-S. Zhou, J. B. Goodenough, H. D. Zhou, K. Matsubayashi, Y. Uwatoko, P. P. Kong, C. Q. Jin, W. G. Yang, and G. Y. Shen, Pressure effect on the structural transition and suppression of the high-spin state in the triple-layer $T'-\text{La}_4\text{Ni}_3\text{O}_8$, *Phys. Rev. Lett.* **108**, 236403 (2012).
- [34] M. Horio, K. Hauser, Y. Sassa, Z. Mingazheva, D. Sutter, K. Kramer, A. Cook, E. Nocerino, O. K. Forslund, O. Tjernberg, M. Kobayashi, A. Chikina, N. B. M. Schröter, J. A. Krieger, T. Schmitt, V. N. Strocov,

- S. Pyon, T. Takayama, H. Takagi, O. J. Lipscombe, S. M. Hayden, M. Ishikado, H. Eisaki, T. Neupert, M. Månsson, C. E. Matt, and J. Chang, Three-dimensional fermi surface of overdoped la-based cuprates, *Physical Review Letters* **121**, 077004 (2018).
- [35] A. Georges and J. Mravlje, Skewed non-Fermi liquids and the Seebeck effect, *Physical Review Research* **3**, 043132 (2021).
- [36] R. S. Markiewicz, S. Sahrakorpi, M. Lindroos, H. Lin, and A. Bansil, One-band tight-binding model parametrization of the high- T_c cuprates including the effect of k_z dispersion, *Physical Review B* **72**, 054519 (2005).
- [37] S. A. Hartnoll and A. P. Mackenzie, Planckian dissipation in metals, *arXiv:2107.07802* (2021).
- [38] H. Jin, A. Narduzzo, M. Nohara, H. Takagi, N. E. Hussey, and K. Behnia, Positive Seebeck coefficient in highly doped $\text{La}_{2-x}\text{Sr}_x\text{CuO}_4$ ($x=0.33$); its origin and implication, *Journal of the Physical Society of Japan* **90**, 053702 (2021).
- [39] J. P. Perdew, K. Burke, and M. Ernzerhof, Generalized gradient approximation made simple, *Phys. Rev. Lett.* **77**, 3865 (1996).
- [40] Z. Li and S. G. Louie, Two-gap superconductivity and decisive role of rare-earth d electrons in infinite-layer nickelates, *arXiv:2210.12819* (2022).